Carbonates dissolution and precipitation in hemipelagic sediments overlaid by supersaturated bottom-waters - Gulf of Aqaba, Red Sea

Zvi Steiner[1,2,*], Boaz Lazar[1], Clare E. Reimers[3], Jonathan Erez[1]

[1] The Fredy and Nadine Herrmann Institute of Earth Sciences, The Hebrew University, Jerusalem 91904, Israel

[2] Department of Earth Sciences, University of Cambridge, Cambridge CB2 3EQ, UK

[3] College of Earth, Ocean and Atmospheric Sciences, Oregon State University, Corvallis, Oregon 97331-5503, USA

* Corresponding Author; email: steinerz@gmail.com

Keywords: calcium carbonate, microelectrodes, dissolution, porewaters, manganese

Abstract

Whether $CaCO_3$ dissolves within the top centimeters of marine sediments overlaid by deep, supersaturated bottom waters remains an area of debate in geochemistry. This uncertainty stems from the fact that different methods used to assess $CaCO_3$ dissolution rates often provide what appear to be profoundly different results. Here we combine microelectrode and porewater chemistry profiles, core incubation experiments, mineral characterizations and observations of the state of preservation of coccolithophorid exoskeletons for a holistic view of carbonate reactions within the top 30 centimeters of hemipelagic sediments from the Gulf of Aqaba, Red Sea. Calculations based on pH and O_2 microelectrode data suggest that rapid metabolic dissolution of carbonate minerals occurs in these sediments within the top two millimeters. Porewater chemistry supports these calculations. The porewater-based observations are further supported by sedimentological characteristics such as aragonite content, and dissolution pitting and fragmentation of coccoliths in sediment layers deposited over the last 200 y. Dissolution appears to be occurring today within surface sediments despite the bulk porewater solution being supersaturated with respect to aragonite and Mg-calcite. In spite of intense dissolution within the sediments, there is no evidence for significant alkalinity and/or calcium fluxes (transport) into bottom waters. It appears that the supersaturated bottom water promotes the removal of all excess alkalinity and calcium produced within the sediment, by $CaCO_3$ precipitation at or above the sediment/ bottom water interface. The precipitation mechanism may be by either benthic organisms (biogenic precipitation) or inorganically (direct precipitation on settling $CaCO_3$ grains). We suggest that authigenic precipitation of

32 $(Ca,Mn)CO_3$ as it becomes supersaturated below 3 cm in the sediments can reconcile the
33 evidence for carbonate dissolution in what appears to be supersaturated conditions. This means
34 that $MnCO_3$ replaces $CaCO_3$ within the nanofossils below ~3 cm, and that part of the
35 manganese rich $CaCO_3$ is bioturbated upwards into undersaturated conditions, facilitating
36 dissolution of these fossils. Diminished calcite and aragonite concentrations in sediments
37 deposited in recent decades are proposed to be a result of increased manganese cycling rates
38 and greater rates of coupled dissolution within the interfacial sediments, possibly combined
39 with diminished calcareous plankton productivity, in response to increased surface water
40 primary productivity.
41

1. Introduction

The ocean is one of the main sinks for anthropogenic CO_2, absorbing 25-30% of present day emissions (Sabine et al., 2004; Le Quere et al., 2018). CO_2 forms a weak acid when it reacts with water, and as such its absorption by the oceans lowers the surface ocean pH, a process termed as ocean acidification (Raven et al., 2005; Doney et al., 2009). This process makes it more difficult for calcareous organisms to build their $CaCO_3$ skeletons (e.g. Feely et al., 2004; Orr et al., 2005; Silverman et al., 2014) and enhances dissolution of $CaCO_3$ minerals in the deep ocean (Ilyina and Zeebe, 2012; Keil, 2017). A significant fraction of the $CaCO_3$ produced in the world ocean, dissolves by CO_2 (as the carbonic acid species) originating from oxygenic remineralization of organic matter in sediments (Archer et al., 1989; Jahnke et al., 1997; Berelson et al., 2007). In deep marine environments, this metabolic dissolution is generally observed in sediments overlaid by undersaturated, or slightly supersaturated with respect to calcite, seawater (Berelson et al., 1990; Hales et al., 1994; Jahnke et al., 1997; Green and Aller, 2001). Whether metabolic dissolution may happen also in sediments overlaid by highly supersaturated bottom waters is still unclear (Broecker and Clark, 2003; Hales, 2003; Jahnke and Jahnke, 2004; Martin and Sayles, 2006). The ambiguity stems from opposing results obtained by the methodologies used in different studies and is complicated by organic and inorganic alkalinity that may be produced in the anaerobic sediment horizons of many deep environments (Table 1). This alkalinity elevates the degree of calcite saturation, and triggers widespread authigenic carbonate mineral precipitation (Sun and Turchyn, 2014). In shallow, supersaturated, marine environments, permeable carbonate sediments generally have high rates of aerobic respiration, little anaerobic remineralization which appears only much deeper under the sediment/bottom water interface, and there is evidence for $CaCO_3$ dissolution in a variety of habitats such as seagrass beds (Hu and Burdige, 2007) and reef clastic sediments and framework (Drupp et al., 2016). Weight loss of biogenic $CaCO_3$ shells was also observed in laboratory experiments with supersaturated, poisoned seawaters (Ries et al., 2016) and in the field around gas seeps with high acidity (Cai et al., 2006).

The full suite of microbial respiration processes that may remineralize organic matter raining onto the sea floor consume oxidants in an order dictated by energy recovery. This order is generally: O_2, NO_3^-, Mn^{4+}, Fe^{3+}, SO_4^{2-}, CH_2O (Table 1; Froelich et al., 1979; Aller, 2014). A reaction stoichiometry for oxidation of organic carbon in an average organic molecule in the presence of oxygen (a simplified version of R1 in Table 1) can be written as:

$$CH_2O + O_2 \rightarrow CO_2 + H_2O \leftrightarrow H_2CO_3 \quad (1)$$

This reaction reduces the pH of the water since CO_2 equilibrates with water to form carbonic acid (Millero, 1995). The excess acid can be neutralized by $CaCO_3$ dissolution by the reaction:

$$CaCO_3(s) + CO_2(aq) + H_2O \rightarrow Ca^{2+} + 2HCO_3^- \quad (2)$$

As more $CaCO_3$ dissolves, the alkalinity of the seawater increases, increasing the water's capacity to hold dissolved inorganic carbon upon equilibration with the atmosphere. The extent to which reactions 1 and 2 co-occur in marine sediments is the extent of metabolic dissolution referred to above and depends on many factors such as the degree of bottom water saturation, properties of the carbonate minerals, and the location of organic matter re-mineralization with respect to the sediment-water interface (Emerson and Bender, 1981). If re-mineralization occurs at the sediment-water interface, a large fraction of the metabolic CO_2 can be released to the water, whereas if it occurs interstitially, the acid has a higher probability of interacting with $CaCO_3$. At the base of the oxic zone, oxygen uptake for re-oxidation of reduced metabolites releases protons and reduces the pH at an even larger rate than aerobic respiration (R6-R9 in Table 1; Jourabchi et al., 2005; Soetaert et al., 2007).

Quantitative studies of early diagenetic processes, such as those that attempt to estimate $CaCO_3$ precipitation/dissolution rates in top sediments, close to the sediment-bottom water interface, "suffer" from methodological bias. As a result, a combination of approaches is recommended for quantitative evaluation of early diagenetic processes (e.g. Broecker and Clark, 2003). The present study combines microelectrode profiles, porewater chemical profiles, core incubations, solid phase analyses and SEM images to: 1. quantify $CaCO_3$ reactions during the early diagenetic history of the northern Gulf of Aqaba (GoAq), Red Sea; and 2. evaluate whether early diagenetic reactions can promote $CaCO_3$ dissolution under supersaturated conditions.

2. Materials and methods

2.1 Study site

The Gulf of Aqaba (GoAq) is characterized by average seawater salinity of ~40.7 g l^{-1}, absence of a significant halocline, and very high bottom water temperatures (>20°C) down to its maximum depth at 1850 m. As a result, GoAq water remains super-saturated with respect to calcite and aragonite at any depth (Krumgalz and Erez, 1984) and pelagic $CaCO_3$ precipitation rates are among the highest observed globally (Steiner et al., 2014). The biological community and physical conditions, on the other hand, have many characteristics of deep water environments. Under these conditions, the kinetics of metabolic and chemical reactions are

very fast due to the high temperatures while the thermodynamic properties of calcite are similar to those found in deep waters (Dong et al., 2018). This allows processes that remain ambiguous in similar water depths elsewhere, to be more pronounced in GoAq. The sites chosen for this study are located at the northern GoAq between 200 and 720 m depth (Fig. 1). The bottom water degree of $CaCO_3$ minerals saturation is >3.5 for aragonite and >5 for calcite, suggesting that carbonate skeletons should be very well preserved. Another important characteristic of the study site, stemming from the weak stratification of the water column, is that at the end of winter, mixed-layer depths extend well below 700 m at least once a decade (Wurgaft et al., 2016). As an outcome of these periodic deep mixing events, much of the water column is re-equilibrated with atmospheric CO_2 and oxygen (Krumgalz et al., 1990). Hence, deep water (700 m) dissolved oxygen concentrations rarely decrease by more than 60 μmol l^{-1} from saturation (Lazar et al., 2008). Vertical mixing of nutrients induces seasonal phytoplankton and macro-algae blooms followed by zooplankton blooms (Lazar et al., 2008). Therefore, GoAq provides an excellent "natural laboratory" for studying the effect of varying organic matter fluxes and increases in the partial pressure of CO_2 on $CaCO_3$ dissolution in deep marine sediments overlaid by bottom waters which are constantly aerobic and highly supersaturated with respect to carbonate minerals.

2.2 Sampling

Sediment cores were retrieved using a 4-barrel multicorer (MC-400, Ocean Instruments, San Diego) from several sites at water depths between 200 m and 720 m in the northern Gulf of Aqaba, Red Sea (Fig. 1). Each core is identified by an eight-digit code, e.g., 720Jan13, in which the first three digits mark the water depth (m), the following three letters mark the month and the last two digits mark the year of retrieval minus 2000. The core tubes (10 cm diameter, 60 cm length) collected 10-37 cm sediment and 50-23 cm of overlying water. Microelectrode profiling and porewater extractions were performed within 14 hours after core recovery, only on cores that maintained clear suspension-free overlying water, throughout the recovery, transport and laboratory setup processes. Nutrient content of the bottom water trapped in the cores and bottom water collected by a rosette sampler were very similar, indicating that porewater of the top sediment was not squeezed out during core retrieval.

2.3 Microelectrodes

Oxygen microprofiles were measured using Clark-type OX-50 sensors (tip size of 50 μm, Unisense, Aarhus) in a laboratory air-conditioned to the bottom water temperature of 21°C.

The sensors were calibrated at air saturation (after bubbling air in a seawater solution for at least 10 min) and at zero oxygen (the lowest steady state electrode reading reached within the sediment over a vertical distance of at least 5 mm). Zero oxygen calibrations were also performed by bubbling N_2 in seawater and in a sodium ascorbate-NaOH solution, but the sensor readings during those calibrations were always higher than the reading at the bottom of the oxic zone. For core 710Nov13, calibration was also performed by bubbling bottom water with N_2 for different time periods and comparing the electrode reading with oxygen determinations using the Winkler method. This produced the expected linear calibration with excellent fit to the standard two-point calibration (supporting figure s1). Oxygen consumption rates and fluxes were calculated using the software PROFILE (Berg et al., 1998) by inputting the mean measured oxygen concentration from each depth in a core along with porosity and bioturbation coefficients calculated from cores from the same site (porosity and bioturbation coefficient at the sediment water interface of these cores was found to be ~0.8 and 0.5-2.5 cm^2 y^{-1}, respectively; Steiner et al., 2016).

Microprofiles of pH were measured with a pH-100 microelectrode (tip size of 100µm) in cores retrieved in 2012 (Unisense, Aarhus) or an amani-1000L PEEK electrode in cores retrieved in 2013 (tip size of 1000µm, Warner Instruments, Hamden, CT), connected to a PHM93 pH meter (Radiometer, Copenhagen). The electrodes were calibrated at 21°C to the NBS scale in three buffer solutions (Radiometer Analytical, Villeurbanne) and immersed in a seawater solution for at least 1 hour before use to equilibrate liquid junction potentials of the electrode and solution. Calculations of the carbonate system parameters from the NBS activity scale were done by the software CO2sys version 2.1 (Pierrot et al., 2006) using the dissociation constants measured by Mehrbach et al. (1973) and refit by Dickson and Millero (1987), and total boron concentration from Lee et al. (2010). Cross calibrations of the pH microelectrodes with a Radiometer pHC2401-7 electrode were performed as quality control. This cross calibration was in perfect agreement with the Unisense electrodes yet the PEEK electrode had significantly different slopes when pH was measured in buffer solutions and seawater. To ensure the long-term consistency of the dataset, calibration of the PEEK electrode was done by calibrating the Radiometer electrode, using it to measure pH in several seawater samples of different pH and then using these seawater solutions as calibration solutions for the PEEK electrode (supporting Fig. s2). Consistency of the pH measurements was assessed by measurements of pH in the overlying water between repeat microprofiles to be ±0.014 pH units (1σ SD, n=15).

Previous benthic respiration studies in other oceans have revealed that core recovery from depths >1000 m may introduce artifacts to measured microprofiles and dissolved oxygen utilization calculations, probably due to core warming and lysis of barophilic organisms (Glud et al., 1994; Epping et al., 2002). Cores for the present study were recovered at water depths that are not considered problematic in terms of the pressure change (Glud, 2008). The unusually high bottom water temperature in the study site (~21ºC) was similar to the room temperature during analyses; hence, core retrieval is not expected to increase the metabolic activity. To minimize random spatial heterogeneity variability in our calculations, each profile presented here is the average of 2-8 microelectrode profiles.

2.3.1 Calculations of $CaCO_3$ dissolution based on microelectrode profiles

Some initial insight into processes controlling pH in pore-waters can be obtained by calculating the expected pH based on oxygen consumption and comparing it with measured values (supporting Fig. s3). This type of calculation is only valid under the restricting assumption that oxygen is the only significant organic matter oxidant. As the concentration of dissolved oxygen decreases with depth, bacterial communities in the sediment may start using other oxidants as electron acceptors (Krumins et al., 2013).

The amount of CO_2 released during organic matter re-mineralization per mole oxidant depends on the oxidation state of the organic carbon being oxidized. In oxic respiration of average marine organic matter, 106 molecules of CO_2 and 16 molecules of nitrate are released for every 138 molecules of O_2 consumed (Redfield, 1958). The lower boundary of the respiratory CO_2/O_2 ratio is 76/138, obtained in the unlikely case that all organic matter being oxidized is in the form of alkanes (Hales et al., 1994). The second factor dictating dissolved inorganic carbon (DIC) accumulation in the pore-water is the ratio between the oxygen and inorganic carbon diffusion coefficients. DIC diffusion is assumed here to be controlled by diffusion of bicarbonate since under normal seawater and interstitial water pH, HCO_3^- accounts for at least 90% of the DIC. Under these assumptions, pore-water DIC concentration at each depth is expressed as (Traub, 1985):

$$\mathrm{DIC} = \mathrm{DIC}_0 + \frac{D_{O_2}}{D_{HCO_3^-}} \cdot \Delta O_2 \cdot \beta \qquad (3)$$

where DIC_0 is DIC at the sediment water interface; $\frac{D_{O_2}}{D_{HCO_3^-}}$, the ratio between the oxygen and bicarbonate diffusion coefficients equals ~2 (Broecker and Peng, 1974; Zeebe, 2011); ΔO_2 is the difference between the oxygen concentration at the sediment-water interface and the concentration at the measured depth; β is the ratio between CO_2 produced and O_2 consumed during organic matter re-mineralization. We limit our assessment of changes in DIC based on oxygen microprofiles to the top 5 mm where dissolved oxygen concentrations are always >50 µmol l^{-1}, implying that oxygen is the major electron acceptor in this zone of the sediment.

During oxic respiration, total alkalinity (A_T) slightly decreases as a result of the oxidation of ammonium to nitric acid and the consequent release of protons and nitrate to the surrounding seawater, at an average ratio of $\frac{\Delta NO_3^-}{\Delta O_2} = -\frac{16}{138}$ (Broecker and Peng, 1982). Assuming no other processes that may change total alkalinity (A_T), e.g. precipitation or dissolution of $CaCO_3$, the change in A_T due to oxygenic respiration would be (Traub, 1985):

$$A_T = A_{T0} - \frac{D_{O_2}}{D_{HCO_3^-}} \cdot \Delta O_2 \cdot \frac{16}{138} \quad (4)$$

where A_{T0} is the total alkalinity at the sediment-water interface.

The amount of $CaCO_3$ (or other carbonate) dissolving in the sediment near the sediment-water interface can be estimated from a change in A_T calculated from the measured pH, DIC derived by Eq. 3 and equilibria relationships in CO2sys software. The difference between this A_T estimate and the A_T estimate obtained from Eq. 4 (alkalinity decrease solely due to nitrate production) is ΔA_T, which is twice the amount of $CaCO_3$ dissolved by production of respiratory CO_2. If the $\left|\frac{\Delta DIC}{\Delta O_2}\right|$ ratio for organic matter oxidation is lower than 106/138 as for alkanes (see above), the calculated ΔA_T reduces by as much as 35%. Furthermore, this calculation does not take into account any increase in DIC as a result of $CaCO_3$ dissolution should near-surface porewaters become undersaturated. An uncertainty of 0.05 pH units in the accuracy of the pH sensor calibration introduces an error of 2 µmol kg^{-1} in calculation of ΔA_T (see supplementary Table s1 for the calculation).

2.4 Porewater separation and porosity

Cores were sectioned at a vertical resolution that ranged from 7 mm at the top of the core to 20 mm near the base within 14 hours from retrieval. Porewater was separated by centrifugation at 5000 rpm for 15 min and filtered through 0.22µm PVDF membranes to remove any remaining solids. Assessments of potential biases in the porewater extraction method employed here suggest that our porewater extraction is reliable for measurements of alkalinity, total dissolved inorganic carbon (DIC), Mn^{2+}, NO_3^- and dissolved silica. pH can be reduced during the separation process by oxidation of Fe^{2+} or elevated due to evasion of CO_2, a problem of greater concern if porewater is extracted in a glove box under a N_2 atmosphere (Steiner et al., 2018a). Sediment porosity was determined from the weight difference between the wet sediment and sediment dried at 60ºC for seven days after porewater separation (Steiner et al., 2016).

2.4.1 Dissolved nitrogen and silica

Dissolved silica (dSi) and total oxidized nitrogen content in porewaters and bottom waters were measured at the geochemical laboratory of the Interuniversity Institute for Marine Sciences in Eilat, using a flow injection auto analyzer (Quick-Chem 8500, LACHAT Instruments, Milwaukee, WI) after dilution at 1:10 ratio with MQ water. Samples for dSi were reacted with molybdate and were subsequently reduced with stannous chloride. dSi concentration was determined by the peak intensity at 820 nm. For determinations of nitrate + nitrite, nitrate was reduced to nitrite by passing the sample through a copperized cadmium column and determining the nitrite with the colorimetric method described by Hansen and Koroleff (1999).

Ammonium concentrations were determined by the method proposed by Holmes et al. (1999) and modified by Meeder et al. (2012) to fit the composition of GoAq seawater. Volumes of 0.25 or 0.5 ml of the separated porewaters were mixed with 3.5 ml distilled water and 1 ml ortho-phthaldialdehyde (OPA). Calibration curves were prepared by spiking filtered, nutrient depleted surface waters to different concentrations of ammonium. The vials were wrapped with aluminum foil, incubated in the dark for three hours and measured with a Hoefer DyNA QuantTM 200 fluorometer (Amersham BioSciences, Little Chalfont). Measurement precision was ±2 µmol l^{-1} (1σ SD, n=20).

2.4.2 Cation chemistry

Samples for dissolved Ca and Mn determination were diluted gravimetrically at 1:70 ratios with 0.16 N HNO_3 and measured at the Institute of Earth Sciences, The Hebrew University, by an ICP-MS (7500 series, Agilent Technologies, Santa Clara, CA) calibrated with multi element standard IV (Merck-Millipore, Darmstadt) and verified with USGS standards T143, T175,

T183 and T199. To correct for instrumental drift, analytical runs were performed with the addition of spikes of internal standards of known concentrations (50 μg L^{-1} Sc and 5 μg L^{-1} Re and Rh), and a consistency standard was run every 5 samples. The samples were run in duplicates and mounted on the ICP-MS in a random order rather than their depth order to verify that observed profiles are not an artifact of uncorrected instrumental drift. Measurement 1σ SD was ±0.8% for dissolved calcium (n=80) and ±2% (n=130) for dissolved manganese determinations.

2.4.3 Carbonate chemistry

Samples weighing 5 g were diluted with equal amounts of milli-Q water then titrated with 0.05M HCl using a Metrohm 716 DMS titrino (Herisau) for total alkalinity determination. Total alkalinity was calculated by the Gran titration method (Sass and Ben-Yaakov, 1977) with a precision of ±10 μmol kg^{-1} (1σ SD, n=250). Calibration and verifications of the measurement accuracy were conducted by titrating in a similar manner a certified reference material provided by Andrew Dickson (Scripps Institution of Oceanography, La Jolla, CA). Dissolved inorganic carbon (DIC) was measured using an AIRICA® DIC analyzer (Marianda, Kiel) connected to a Li-6252 IR-CO_2 sensor (LI-COR, Lincoln, NE) in samples poisoned by adding 1% of saturated $HgCl_2$ shortly after porewater separation. A certified reference material provided by Andrew Dickson was run every 4 samples and used for calibration and drift corrections. pH of the separated porewaters was measured with a PHM64 research pH meter (Radiometer, Copenhagen) equipped with a PHG201-7 glass pH electrode with a REF201 reference electrode at 25°C. Internal precision of the measurements was better than 0.005 units as reflected by duplicate analyses of the same samples.

The saturation state of the main carbonate minerals was calculated based on cation chemistry, dissolved silica, dissolved nitrate, dissolved orthophosphate and carbonate chemistry data. Apparent saturation constants of calcite and aragonite used for these calculations are from Mucci (1983) and of rhodochrosite from Johnson (1982). The stoichiometric saturation constant of high Mg-calcite used here is the fit to biogenic Mg-calcite containing 12 mol% $MgCO_3$ as drawn by Morse et al. (2006), modified according to the temperature and salinity dependence drawn for calcite by Mucci (1983). Pressure corrections of the saturation constants follow Millero (1995) and Lewis and Wallace (1998). It was assumed for the calculations that pressure dependence of Mg-calcite and rhodochrosite saturation constants follow the pressure dependence of calcite saturation. The carbonic acid dissociation constants used for these

calculations are from Mehrbach et al. (1973). Total ion activity coefficients of CO_3^{2-}, Ca^{2+} and Mg^{2+} used for calculations of Mg-calcite saturation were calculated using PHREEQC 3.1.5 (Parkhurst and Appelo, 2013).

2.5 Core incubations

Dissolved silica, nitrate + nitrite (NO_3^- + NO_2^-; appears in the figure legends as NO_3^- since concentration of nitrate we measure in the cores is always more than an order of magnitude higher than concentration of nitrite), total alkalinity, O_2 and pH were monitored in the overlaying waters every 6-8 hours for several days after core recovery. Cores used in these incubations were stored sealed in the dark at bottom water temperature. During these experiments, seawater was recirculated at a rate of 20 ml per minute using a peristaltic pump, by pumping out at ~5 cm above the sediment-water interface and pumping in at the top of the water column. Control experiments without recirculation were conducted. In both cases, seawater sampling was followed by replenishment from an external reservoir which contained bottom water collected using a Niskin bottle from the same depth as the core. The flux of a dissolved species monitored during incubation experiments was calculated as the rate of change in concentration in the overlying water, corrected for the overlying water volume and dilution due to water replenishment and normalized to core surface area. Analytical chemistry protocols were similar to the porewater analyses except that dilution was not required for total alkalinity and nutrient determinations.

2.6 Solid sediment

Coccolithophore abundance and preservation states were qualitatively assessed using high resolution scanning electron microscopy (HR-SEM) images obtained by a Magellan-400L (FEI, Hillsboro, OR) at the Hebrew University Unit of Nanocharacterization.

Further analyses were conducted on samples that were first dried and crushed with mortar and pestle. X-ray diffraction spectra were obtained by a D8 Advance diffractometer (Bruker AXS, Karlsruhe) equipped with a secondary graphite monochromator, 2˚ Sollers slits and 0.2 mm receiving slit. A low-background quartz sample holder was carefully filled with the powder samples. Measurements were carried out at room temperature using CuKα radiation (λ=1.5418 Å) with tube voltage of 40 kV and tube current of 40 mA. Sample scanning was conducted at step-scan mode within the range 5˚ to 65˚ 2θ with a step size of 0.02˚ 2θ and counting time of 1 s/step. Instrumental broadening was determined using LaB_6 powder (NIST SRM 660).

Mineral identifications and calculations of their relative content were conducted using EVA 3.0 software based on all observable peaks.

Carbonate mineral content of the bulk sediment was determined using a "carbonate bomb" by reacting 1 g of sediment with 5 ml distilled water and 1.2 ml concentrated HCl in a closed vessel for five minutes while shaking. Pressure inside the vessel before the acid contacted the sample was subtracted from the pressure after the reaction ceased to determine pressure buildup due to CO_2 release. Calibration curves were prepared by reacting different amounts of pure $CaCO_3$ powder in the same way. The fit between $CaCO_3$ powder weight and the CO_2 pressure in the cell was linear with R^2=0.9999. Measurement precision was ±0.2% (2σ SD, n=30).

Splits of 250 mg of the dried and powdered sediment samples were leached with 10 ml of 4M HNO_3 at 80°C for 16 hours. The acid was subsequently diluted 1:40 and analyzed with an ICP-MS (7500 series, Agilent Technologies, Santa Clara, CA) using similar procedures to those described in section 2.4.2.Core 520May12, the main core we use for solid state analyses in the present study, was previously dated using measurements of excess ^{210}Pb activity and changes in planktonic foraminifera abundance (Steiner et al. 2016). The planktonic foraminifera dating was based on numerous observations that *Globogerinoides sacculifer* was the most abundant planktonic foraminifera species in this region throughout the Holocene and until ~1990 as determined from sediment cores and plankton net tows. Since 1990, *G. sacculifer* was not found in plankton net tows from this region while *Orbulina universa,* which was previously very rare in this region, started to appear in significant numbers. This change can be seen in recent sediment cores and was used by Steiner et al. (2016) to calculate sedimentation and bioturbation rates. In core 520May12, sedimentation rates calculated by both dating methods are in excellent agreement (~1 mm y^{-1}).

3. Results

3.1 Microelectrodes profiles

Oxygen penetration depths in the various cores studied here were 11-18 mm (Fig. 2), similar to the oxygen penetration depths reported by Boyko et al. (2018) in cores retrieved in September 2016 from the same region. Calculated volumetric oxygen consumption rates are highest near the sediment water interface and decrease downward, with no apparent increase in oxygen consumption rates near the oxic-anoxic boundary. The deeper cores seem to have deeper oxygen penetration depths but also higher oxygen consumption rates, especially near

the sediment-water interface. This trend is particularly pronounced in core 710May12 where a threefold increase in the calculated oxygen consumption rate is found at the top 1.5 mm of the sediment (Fig. 2). This core was retrieved shortly after an exceptionally deep winter mixing event that ventilated the entire water column and induced a strong spring bloom (Wurgaft et al., 2016).

Based on the organic matter oxidation series, it is anticipated that pH should decrease in the oxic zone and increase when manganese and iron oxides are used for organic matter oxidation (Froelich et al., 1979). The maximum rate of acid production often occurs at the base of the oxic zone when oxygen reacts with reduced manganese, iron and ammonium (Canfield et al., 1993; Burdige, 2006; Aller, 2014). Measured pH microprofiles from our cores indeed follow this predicted sequence yet the slope of the change in pH with depth and the location of the minimum vary among the different cores (Fig. 3). Despite these marked differences, the minimum pH value in all cores was very similar, suggesting a strong carbonate buffer that stops pH_{NBS} from falling well below 7.6.

Plots of calculated excess total alkalinity, ΔA_T (the difference between the alkalinity calculated from the mean measured pH and calculated DIC by Eq. 3, assuming that organic matter oxidation follows Redfield ratios of $\frac{\Delta DIC}{\Delta O_2} = -\frac{106}{138}$, and the alkalinity calculated by Eq. 4 from the dissolved oxygen profile), indicate that a carbonate mineral dissolves within the uppermost 2 mm of all four cores measured by microelectrodes. The slopes of all ΔA_T profiles in the different cores are similar and quite linear within the top 2 mm (Fig. 4), despite differences in oxygen consumption rates (Fig. 2). Similar alkalinity accumulation in the top 2 mm of all studied cores suggests that near-surface dissolution rates of carbonate minerals are not very sensitive to variations in spatial and temporal respiration rates. A_T production rates in the top 2 mm calculated by the software PROFILE (Berg et al., 1998), inputting calculated ΔA_T and assuming that transfer of alkalinity is by diffusion of HCO_3^- ions, are 0.013±0.009 nmol cm^{-2} s^{-1}, and calculated fluxes to the bottom waters are 2.5±0.5 mmol m^{-2} d^{-1}. The dissolution of carbonate minerals produces 2 moles of alkalinity for each mole of carbonate minerals dissolved, hence this calculation suggests a dissolution flux of ~1.2 mmol m^{-2} d^{-1}. It should be noted also that the steeper decrease in pH following the 2012 winter mixing event (Fig. 3) was not accompanied by a steeper ΔA_T when compared with other cores (Fig. 4). The almost linear ΔA_T trend may suggest that most of the dissolution occurred at the bottom of the 2 mm top layer, and the dissolution signal is diffused upward to bottom water. The diversion between

different profiles below ~3 mm may suggest that deeper in the sediment, oxygenic respiration is not the sole process responsible for oxidation of organic matter.

3.2 Porewater profiles and link to the bottom water

Porewater profiles of dissolved Mn show very clear spatial difference: a marked, factor of 10, increase in dissolved Mn as a function of bottom depth, from ~10 μmol kg^{-1} at 200 m depth to ~100 μmol kg^{-1} at 720 m (Fig. 5). The redox control on precipitation/dissolution of Mn-minerals is reflected by the marked decrease in dissolved Mn at the upper sediment layer, in which it is oxidized by O_2 and precipitates as MnO_2. When oxygen is consumed for the re-oxidation of reduced anaerobic metabolites, less oxygen is available for oxygenic re-mineralization of organic matter (Canfield et al., 1993). Considering that these reactions release protons and reduce the pH at a higher rate than oxic respiration (R6-R9 in Table 1), carbonate mineral understaturation can occur even if all oxygen is consumed by the oxidation of reduced metabolites.

Comparing measured porewater alkalinity profiles (Fig. 6) with porewater dissolved manganese (Fig. 5), supports the idea that oxidation of organic carbon and reduced metabolites enhances dissolution at the base of the oxic zone. The near surface alkalinity show an increase with depth in all cores. Below this initial increase the profiles diverge, in most cores, total alkalinity reaches a maximum and decreases again with depth down to a local minimum. In the cores 400Aug11 and 578Jan12 this minimum is located very shallow and its alkalinity value was lower than that of the bottom water, suggesting a significant carbonate sink at that depth. In most cores from ~700 m, porewater Mn concentrations increase to ~100 μmol kg^{-1} at 4-5 cm (Fig. 5A), while at the same core depths total alkalinities were at a local maximum (Fig. 6A-D). Following this peak, alkalinity decreases downward reaching a minimum at ~10 cm, with a value similar to that of bottom water. Alkalinity produced deeper then ~10 cm is therefore consumed within the sediment layer above. A substantial increase in the degree of rhodochrosite supersaturation supports that the precipitated phase is probably a manganese carbonate (Fig. 7D). Calcite remains supersaturated when $MnCO_3$ precipitates (Fig. 7A), hence it seems likely that the precipitating mineral phase is mixed $(Ca,Mn)CO_3$ rather than pure $MnCO_3$ (Middelburg et al., 1987; Mucci, 1988).

The deeper layers of the sediments are a sink for dissolved calcium (Fig. 8). Decreased dissolved Ca^{2+} concentrations below the first few cm correlates with increased $CaCO_3$ content below 15 cm (Fig. 9A). The possibility that widespread precipitation of secondary $CaCO_3$

accounted for the increase in $CaCO_3$ content with depth was rejected after visual inspections of the sediments under a light microscope and SEM.

A final approach we have taken to verify the accuracy of the porewater and microelectrode based dissolution estimates was to follow the concentrations of the carbonate system constituents in the overlying water during several days of incubation. These incubations show a clear and gradual decrease in the pH of the overlying water due to organic matter re-mineralization (Fig. 10C) while measured total alkalinity concentrations remain stable (Fig. 10D). Correcting measured total alkalinity data from the incubations for changes in nitrate concentrations during the experiment (Fig. 10B) remove most of the signal, other than a small increase at the end of the core 400Aug11 experiment. This suggests that there is no net flux of alkalinity from the sediments to the water column.

3.3 Solids

HR-SEM images of the <63 μm fraction of core 520May12 (Fig. 9C-L) reveal a qualitative relation between measured carbonate content (reported as $CaCO_3$ weight %) and the abundance of coccolithophorid remains. A good correlation is observed between aragonite and total carbonate content, particularly towards the core top (Fig. 9B). At the bottom part of the core, $CaCO_3$ content is >35% (Fig. 9A), coccoliths comprise a significant fraction of the sediment and are very well preserved (Figs. 9K-L). Coccolith abundance decreased together with the decrease in the $CaCO_3$ content toward the end of the 19th century, yet they remained a major component of the <63 μm size fraction. The coccolith state of preservation also deteriorated at that point (Fig. 9I-J).

A pronounced decrease in coccoliths abundance, their state of preservation and $CaCO_3$ content is observed in the sediment layer deposited during the late 1990's and early 2000's (Fig. 9E-F; 0.5-1.5 cm depth). This period was characterized by elevated nutrient fluxes to the northernmost part of the Gulf of Aqaba due to fish farming activity and increased surface water productivity (Lazar et al., 2008; Black et al., 2012; Steiner et al., 2017). In this layer, coccoliths are nearly completely absent; only rare specimens in a very poor state of preservation are detected (Fig. 9E shows the best-preserved specimen we found in this layer). Coccoliths reappear in the surface sediment and are much better preserved, yet close inspection reveals that intensively dissolved specimens are found near pristine ones (Fig. 9C). These observations point to significant dissolution intensity in the oxic zone since calcite plates precipitated by coccolithophores are usually highly resistant to dissolution, even compared to other low

magnesium calcite skeletons like those produced by planktonic foraminifera (Chiu and Broecker, 2008).

Manganese concentrations in the sediment increase as a function of water depth in the northern Gulf of Aqaba (Fig. 11), in agreement with the porewater data (Fig. 5). The increase in solid phase manganese concentrations in the top 2 cm is probably the result of oxidation of Mn^{2+} to Mn^{4+} and precipitation of manganese oxides in the oxic part of the sediment. The continued enrichment in manganese below the manganese reduction zone in core 690Jun11 (Fig. 11) suggests that much of the Mn^{2+} produced by microbial respiration is adsorbed to the sediment or retained in carbonate minerals.

4. Discussion

4.1 Calcareous skeleton abundance and carbonate preservation in the sediments

Visual evidence of coccolith dissolution (Fig. 9) supports calculations based on microelectrode and porewater data pointing to significant carbonate dissolution during the early stages of diagenesis (Figs. 4, 6), despite high bottom water supersaturation in the study site (Fig. 7). A strong correlation between aragonite and total carbonate mineral content (Fig. 9B) is indicative of the important role of pteropods in $CaCO_3$ productivity and/or preservation in the Gulf of Aqaba. Previous studies from this region showed that aragonite skeletons of pteropods can undergo dissolution in Red Sea and Gulf of Aqaba sediments (Traub, 1985; Almogi-Labin et al., 1998). Dissolution signs were also observed in the more robust calcite skeletons of planktonic foraminifers (Sultan, 2014).

The observed increase in $CaCO_3$ dissolution intensity toward the present, peaking in the first decade of the 21^{th} century, suggests that a significant increase in metabolic acid production within the sediment occurred as water column productivity increased. Improved preservation of coccoliths shells in the top sediment as well as the qualitative agreement between aragonite and coccolith content of the sediment, suggest that dissolution may have played a role in producing the near surface $CaCO_3$ minimum found in these cores. Based on the SEM images (Fig. 9), we note that most coccoliths reach the sediment within fecal pellets. Therefore, their preservation also depends on the metabolic state of their predators (Harris, 1994). At the same time, the general trend of decreased carbonate preservation toward core tops is in agreement with the expected effects of progressive ocean acidification (OA). It should be noted that the top sediments of the deep water of the northern Gulf of Aqaba can serve as a sensitive proxy

for ongoing OA, because the water column is mixed completely at least once a decade, transporting the OA signal (e.g. lowering Ω of bottom water) down to the bottom. During 1998-2018, total alkalinity has increased in the Gulf of Aqaba due to decreased calcification rates in the Red Sea and Gulf of Aqaba (Steiner et al., 2018b). The increase in total alkalinity countered the effect of increased partial pressure of carbon dioxide and kept the saturation state for carbonate minerals nearly constant (Steiner et al., 2018b).

The late 19th century change in Gulf of Aqaba $CaCO_3$ cycle recorded in these sediments is in temporal agreement with sedimentary data from the Indian Ocean, suggesting weaker upwelling due to decreased monsoon intensity during the little Ice Age (Gupta et al., 2003). The Indian Ocean is the only significant natural source of water and nutrients to the Gulf of Aqaba via a double distillation system which only allows passage of nutrient deplete surface waters through the shallow straits of Bab el Mandeb and Tiran (Sofianos and Johns, 2002; Biton and Gildor, 2011). Important nutrient sources in such oceanographic setting are their input with surface water particulate organic matter (POM) in the form of phytoplankton, zooplankton, TEP, etc. This nutrient input may had decreased markedly due to the weakening of the Indian monsoon that was most probably accompanied by decreased productivity. This setting may had resulted in increased abundance of coccolithophores relative to faster growing algae such as diatoms as well as decreased metabolic acid (CO_2) production rates within the sediments during the little Ice Age.

4.2 $CaCO_3$ dissolution in supersaturated conditions

The apparent contradiction observed in this study, in which microelectrode and porewater data suggest net dissolution of carbonate minerals near the sediment-bottom water interface (Figs. 4, 6), but core incubations show no evidence for that process (Fig. 10), was previously reported in study from the Ceara Rise (Hales and Emerson, 1997; Jahnke and Jahnke, 2004). To explain this contradiction, Broecker and Clark (2003) suggested that in sediments overlain by supersaturated bottom waters, metastable $CaCO_3$ phase may precipitate at the sediment/water interface and dissolve back when buried (either by sedimentation or bioturbation) deeper by metabolic acids. The ability of the supersaturated open water column of the Red Sea and Gulf of Aqaba to precipitate carbonate minerals by heterogeneous precipitation on suspended inorganic particles was demonstrated by Wurgaft et al. (2016). Similarly, it is very likely that heterogeneous precipitation of $CaCO_3$ occurs at the sediment-bottom water interface of the Gulf of Aqaba, which serves as an extremely good contact zone between supersaturated

seawater and particles. Another likely source for $CaCO_3$ precipitation at or above the sediment-water interface is skeleton formation by benthic organisms (e.g. benthic foraminifera, Mollusca, echinoderms). Many of these organisms live on the sediment surface, having minimal effect on porewater profiles.

An alternative explanation for this phenomenon is that carbonate dissolution in the upper part of the sedimentary column in the Gulf of Aqaba is linked to internal cycling of manganese. Reduction of manganese oxides below the oxic-anoxic interface increases porewater concentrations of Mn^{2+} (Fig. 5) bringing $MnCO_3$ to supersaturation below 3 cm (Fig. 7D) and inducing authigenic precipitation of Mn-carbonates (Fig. 6A-D). Bioturbation coefficients at the study site are two orders of magnitude lower than molecular diffusion coefficients of dissolved substances (Steiner et al., 2016), yet they are high enough to mix part of the authigenic $MnCO_3$ back to the surface. The contact of this solid $MnCO_3$ with surface sediment porewater which is undersaturated with respect to rhodochrosite should induce $MnCO_3$ dissolution within the uppermost 2 mm as calculated from the microelectrode data. Mn^{2+} released in the process (Fig. 5) is rapidly oxidized to MnO_2 by dissolved oxygen (Fig. 2).

Apparently, the model suggested above does not fit the evidence that nanofossil dissolve (Fig. 9) and the widespread occurrence of calcite and aragonite dissolution in the supersaturated conditions of the deep water of the Gulf of Aqaba. Two possible mechanisms maybe responsible for this observation: 1. The ballasting effect which cause planktonic $CaCO_3$ skeletons to sink fast to the sediments, while still "full" with their organic matter (Armstrong et al., 2002; Klaas and Archer, 2002, Engel et al, 2009). When their internal POM oxidized, it creates $CaCO_3$ undersaturated micro-environments in contact with $CaCO_3$ surfaces (Freiwald, 1995); and 2. Part of the Ca in these fossil skeletons is replaced by Mn at the sediment interval in which the concentration of dissolved Mn increases. The chemisorption of Mn^{2+} onto $CaCO_3$ surfaces followed by substitution of Ca in the lattice was previously shown to be much faster than precipitation of rhodochrosite because Mn has a much higher affinity to $CaCO_3$ surface than Ca (McBride, 1979; Wartel et al., 1990). Shells comprising $Mn_x,Ca_{1-x}CO_3$ are prone to dissolution when transported by bioturbation to the surface of the sediment (Fig. 7D).

We prefer mechanism #2 (Ca replacement by Mn) because it is very likely that the eutrophication of the Gulf of Aqaba in recent decades (Lazar et al., 2008; Steiner et al., 2017) enhanced the rates of manganese metabolism and bioturbation. Intensive dissolution of $CaCO_3$ within patchy, organic matter rich, microenvironments should have produced scattered micro

pH profiles. The relatively smooth profiles we measured (Fig. 3) suggest that dissolution in microenvironments is not the dominant mechanism in this case.

4.3 Synthesis

This study provides evidence for precipitation/dissolution of carbonates in the top ~30 cm (with special emphasis on the top several centimeters) of a marine sedimentary section overlaid by warm, well oxygenated water column supersaturated with respect to calcite, aragonite and Mg-calcite and mostly undersaturated with respect to rhodochrosite. The data was obtained from cores taken in the northern Gulf of Aqaba, Red Sea, using four different approaches: 1. Laboratory microelectrode profiles in the upper three cm of the sediment; 2. Profiles of porewater chemistry; 3. Temporal variations in seawater chemistry of waters overlaying the sediment-water interface of laboratory incubated cores; and 4. Mineral characterizations and qualitative assessment of the state of preservation of coccolithophorid exoskeletons. The data provided several apparently contradicting results, which led us to the following conclusions regarding the link between redox state, degree of mineral saturation and solids and porewater vertical transport (by either bioturbation or diffusion):

1. All microelectrodes profiles suggest that carbonates dissolve rapidly within the top ~2 mm of the sediment column, producing alkalinity at a rate of 0.013±0.009 nmol cm^{-2} s^{-1}. The dissolution rates are rather constant and not affected by either season or oxygen consumption rates.
2. Carbonates dissolution intensity in Gulf of Aqaba sediments is high enough to attack stable biogenic calcites and not just metastable forms of calcium carbonate. This is an extremely important finding regarding the preservation of carbonate minerals in the top most sediments of marine environments containing porewaters (and bottom waters) supersaturated with respect to calcite, Mg-calcite and aragonite.
3. Authigenic $CaCO_3$ precipitation occurs below 10 cm in the sediments (as indicated by porewater calcium profiles).
4. The oxidation of reduced metabolites by dissolved oxygen at the base of the oxic zone, such as Mn^{2+} in the cores sampled below 500 m depth (Figs. 5A, B), produces an additional acid source, which facilitates further carbonate mineral dissolution. Oxygenic oxidation of Fe^{2+} produces the same effect, but at this particular site, Fe^{2+} maximum concentrations and its upward flux are often lower than those of Mn^{2+} (Blonder et al., 2017).

5. The high concentrations of Mn^{2+} in porewater from sediments deeper than 500 m may potentially trigger precipitation of $MnCO_3$ below 3 cm in the sediment (Fig. 7D). This $MnCO_3$ may re-dissolve upon being "bioturbated" to the undersaturated surface sediments.
6. Despite evidence for $CaCO_3$ dissolution within the sediments, the bottom water does not record a carbonate dissolution signal. Excess alkalinity and calcium produced within the sediment is removed by carbonate mineral precipitation at or above the sediment/ bottom water interface by either benthic organisms or inorganically. Inorganic removal of alkalinity could proceed by direct precipitation as coating on $CaCO_3$ grains or due to "buffer" for alkalinity escape, induced by internal recycling of solid $MnCO_3$ and $Mn_xCa_{1-x}CO_3$. In this scenario, the dissolution of $MnCO_3$ phases that were "bioturbated" to the surface sediment layer, triggers subsequent oxygenic oxidation of the released Mn^{2+} to precipitate highly insoluble solid MnO_2 preventing alkalinity of escaping across the sediment-water interface.
7. The phenomena described in this study may stem partly from the long and short term variations in the oceanographic conditions in the northern Red Sea. Increased productivity and nutrient load to the Gulf of Aqaba region due to anthropogenic activity (Lazar et al., 2008; Steiner et al., 2017) during the end of the 20th and beginning of 21st centuries, as well as the intensifying effects of ocean acidification and change in the monsoon regime may be responsible for these variations. This may explain the decrease in the state of calcareous skeleton preservation over the past 200 y and particularly over the past two decades.

Acknowledgements

This study was funded by the University of Calgary CCS initiative grant to JE. ZS was supported by an Eshkol fellowship from the Israeli ministry of Science and Technology, a research grant from the Interuniversity Institute for Marine Sciences in Eilat (IUI) and a Blavatnik post-doctorate fellowship. We thank Alexandra Turchyn and Chin-Yik Lin for reading and commenting on previous drafts of this paper. We thank the staff of the IUI: Timor Katz, Sefi Baruch, Asaph Rivlin and Moti Ohavia for assisting with the field work and Tanya Rivlin for conducting the nutrient measurements and assisting with lab work. We thank the staff of the Hebrew University: Ofir Tirosh (Institute of Earth Sciences) for assisting with ICP-

606 MS analyses and Vitaly Gutkin and Vladimir Uvarov (Unit of Nanocharacterization) for
607 assisting with the SEM imaging and XRD analyses.

608 # Figures and tables

609

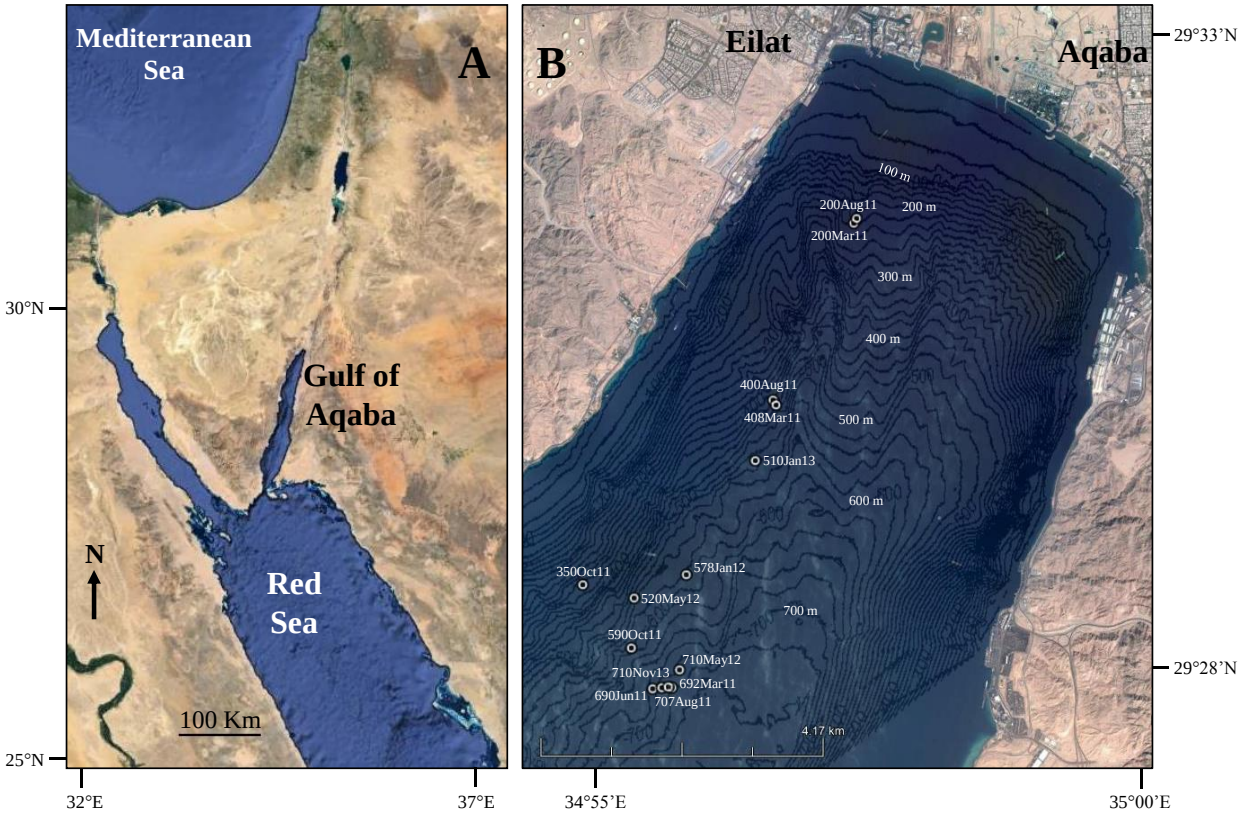

610

611 **Fig. 1:** Google Earth images of the study area. (A) Regional map. (B) Zoom in on the study
612 region showing the locations of cores retrieved for the present work. 20 m isobaths were drawn
613 based on the survey of Tibor et al. (2010).

614

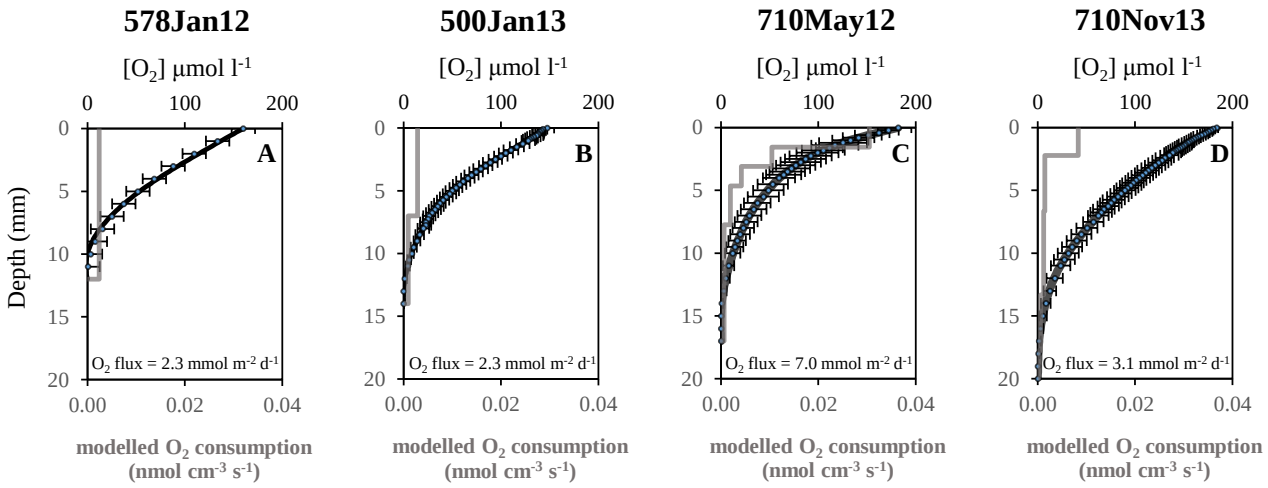

615

616 **Fig. 2:** Microprofiles of dissolved oxygen and the calculated oxygen consumption rates in four
617 different dates during 2012 and 2013. Circles stand for the average oxygen concentration
618 measured at the same depth in different profiles from the same core, error bars mark the average
619 deviation of the different profiles from the mean, the solid black lines are the model fit to the
620 data. O_2 consumption rates (solid grey lines) and dissolved oxygen fluxes at the sediment-water
621 interface were calculated using the software PROFILE (Berg et al., 1998).

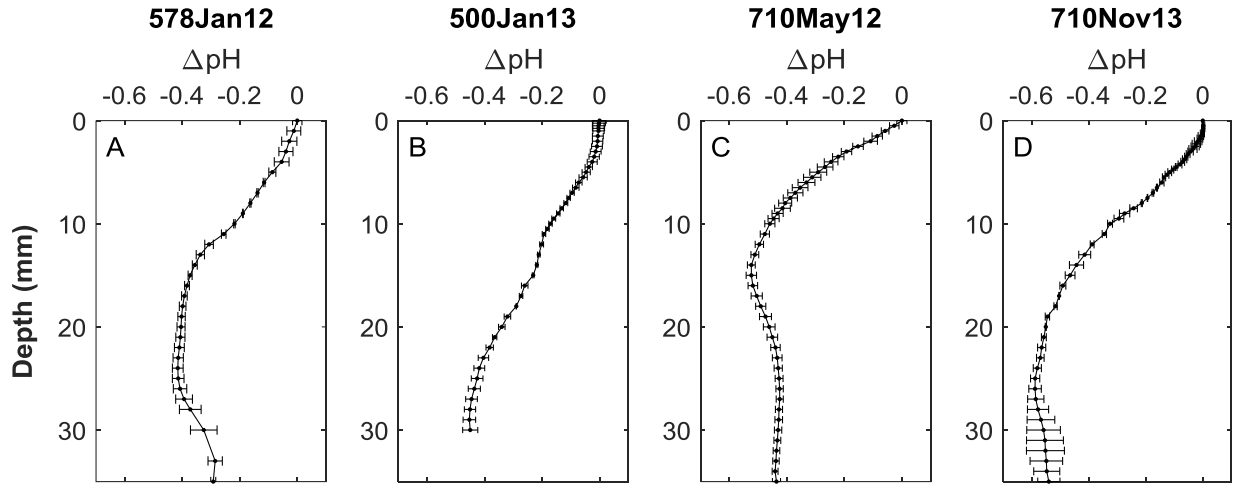

622

623 **Fig. 3**: Vertical profiles of the differences between the measured pH and the pH at the sediment
624 water interface. Error bars mark the average deviation from the mean of different profiles from
625 the same core.

626

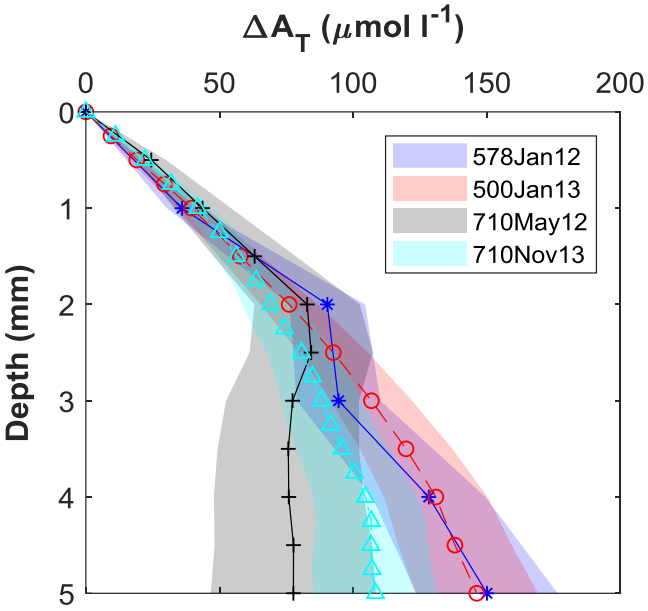

627

628 **Fig. 4:** Calculated excess total alkalinity (ΔA_T) as a proxy for carbonate mineral dissolution
629 based on the oxygen and pH microelectrode data. The colored uncertainty ranges for each
630 profile reflect a possible range in $\frac{\Delta DIC}{\Delta O_2}$ ratios: The lowest ΔA_T vs. depth for each profile was
631 calculated from $\frac{\Delta DIC}{\Delta O_2} = -\frac{90}{138}$ and the highest from $\frac{\Delta DIC}{\Delta O_2} = -\frac{122}{138}$.

632 *578Jan12; O500Jan13; +710May12; Δ710Nov13.

633

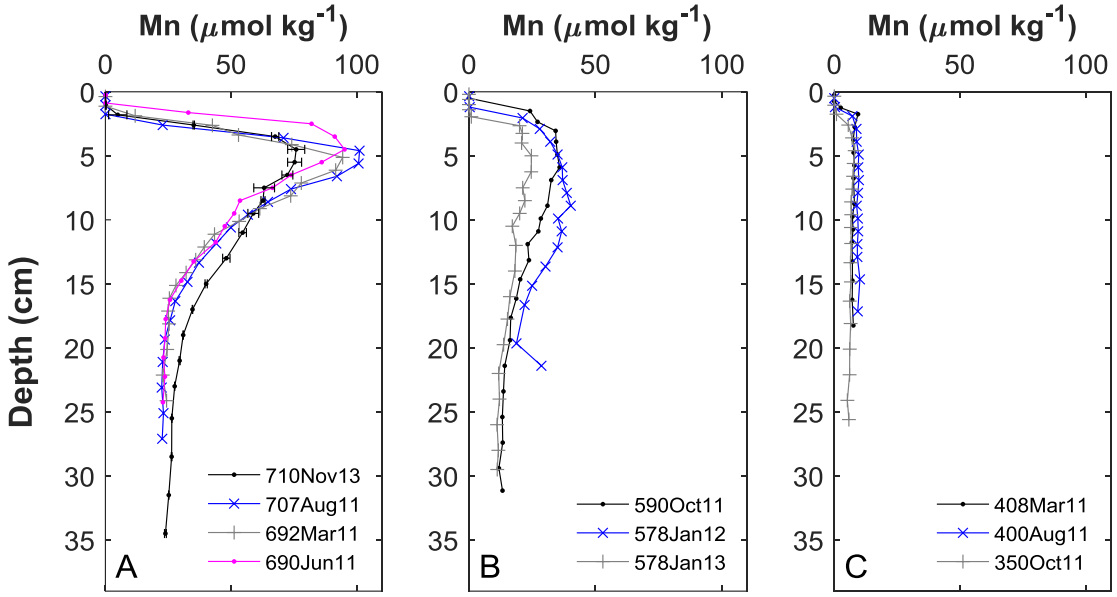

634

635 **Fig. 5:** Profiles of dissolved manganese concentrations versus depth in the studied cores at
636 three different bottom depths: A- depth ~700 m; B- depth ~600 m; C- depth ~400 m.
637 Analytical precision was ±2% (1σ SD, n=130, plotted for core 710Nov13).

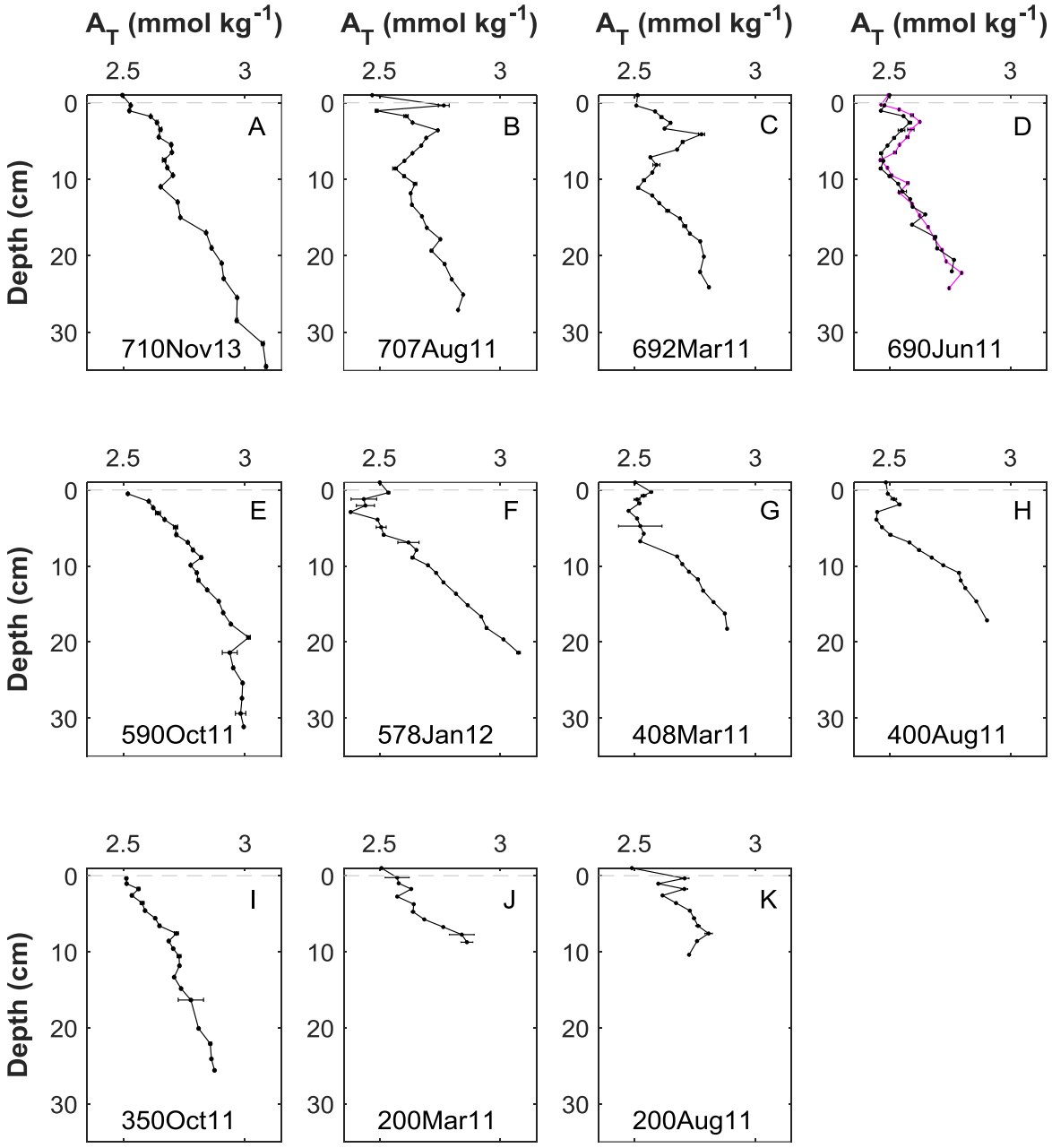

638

639 **Fig. 6:** Depth profiles of porewater alkalinity. Two profiles in 690Jun11 refer to analyses on
640 porewaters extracted from two cores from the same cast. Analytical error is normally smaller
641 than the symbol size. Error bars mark the average deviation between duplicate analyses in the
642 few samples where this deviation was larger than the symbol size.

643

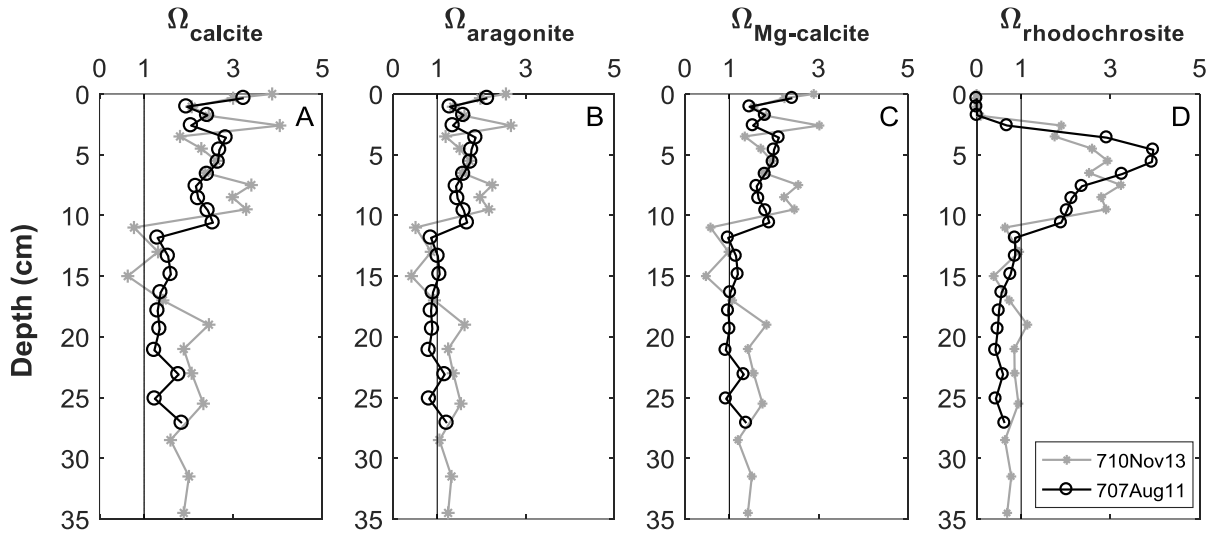

644

645 **Fig. 7:** Profiles of the saturation state, Ω (the ion activity product divided by the thermodynamic
646 solubility constant), of the main carbonate minerals in the porewaters of core 707Aug11 (black
647 line; calculated from A_T and pH data) and 710Nov13 (gray line; Ω calculated from A_T and DIC
648 data). Chemical analyses were conducted on porewater extracted by centrifugation. The
649 vertical line marks Ω=1 (saturation with respect to the specific solid carbonate phase).

650

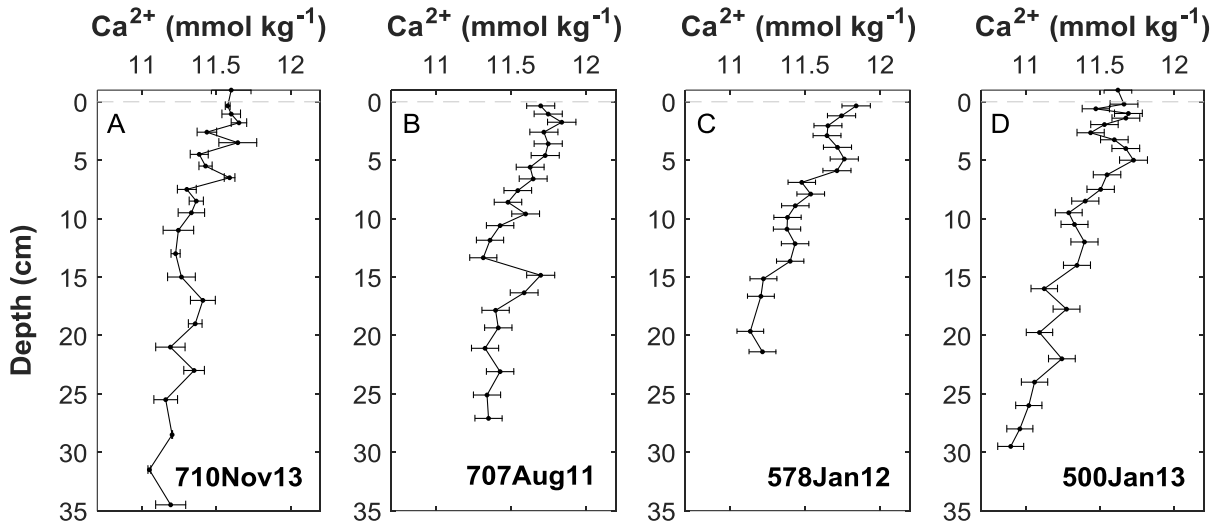

651

652 **Fig. 8:** Profiles of porewater dissolved calcium concentrations. Error bars mark the average
653 deviation between duplicate analyses in core 710Nov13 or 0.8% in other cores.

654

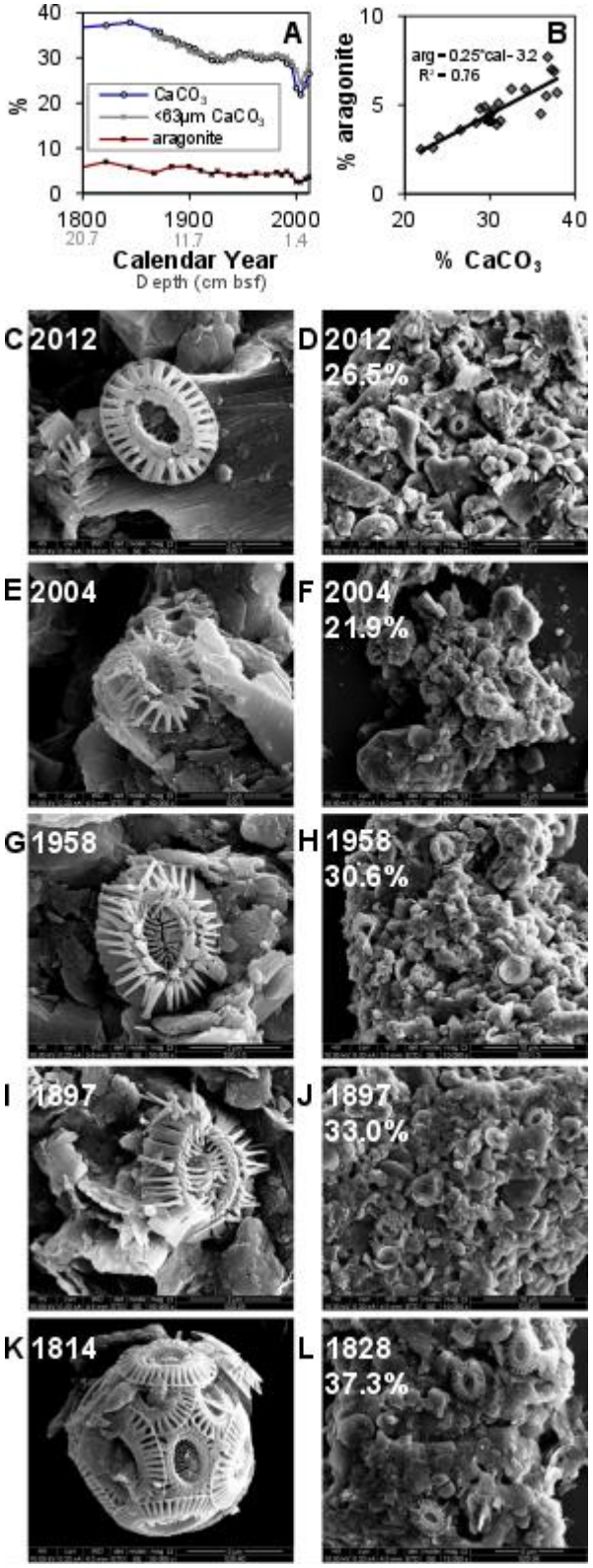

Fig. 9: Variations in $CaCO_3$ composition of core 520May12. A- carbonate mineral content of the bulk sediment (assumed to be dominated by $CaCO_3$), the fraction smaller than 63µm and aragonite content of the bulk sediment. The x-axis shows the calendar years as calculated by the age model of Steiner et al. (2016) and the depth in the core (grey fonts). B: Correlation between bulk sediment %$CaCO_3$ and aragonite content. C-L: HR-SEM images of the <63µm fraction. Numbers indicate calculated mean calendar age of the sample and % $CaCO_3$ of the bulk sediment. Left column images show the preservation state of *E. huxleyi* remains. Right column images show the composition of fecal pellets. Images C, E, G and I were magnified X50,000; images D, F, H and J X10,000; image K X35,000 and L was magnified X15,000.

655

656

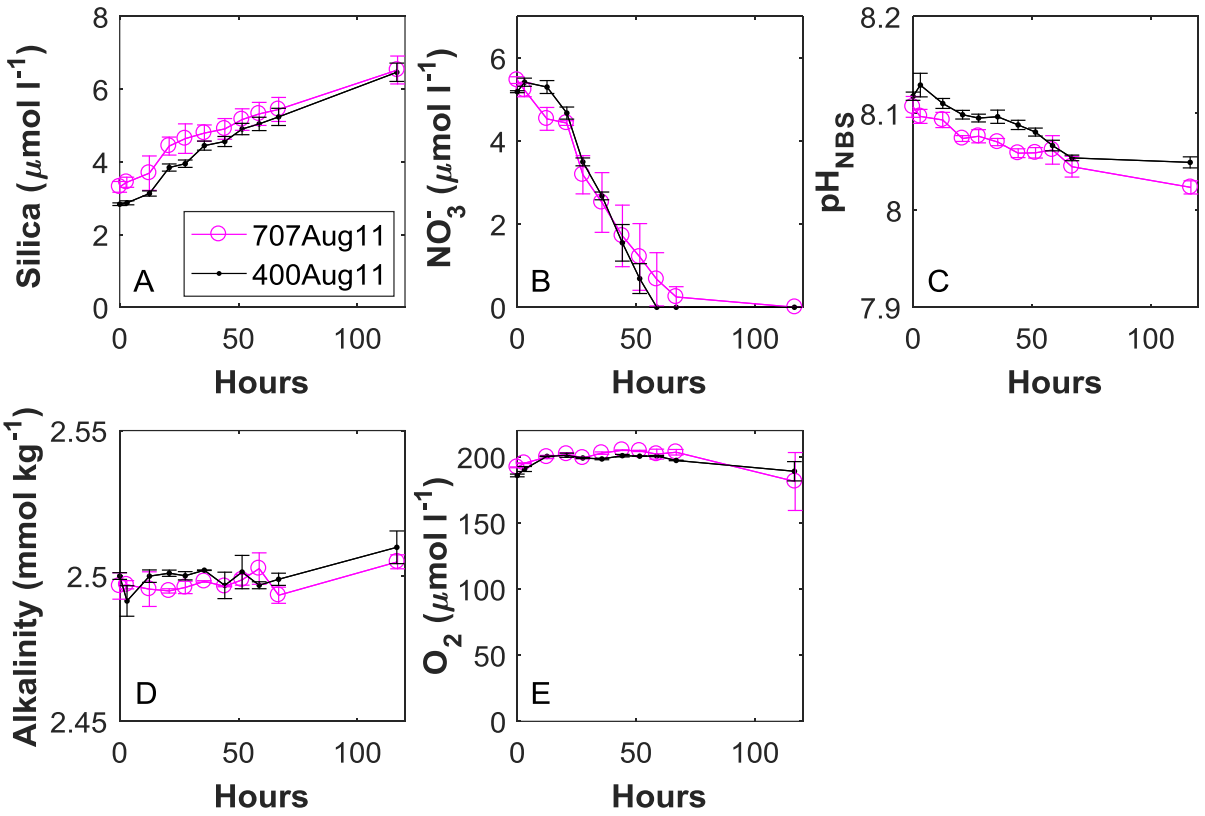

657

658 **Fig. 10:** Concentrations of dissolved analytes in the overlying water of cores incubated during
659 5-days in August 2011. Each point is the average of two cores from the same multicorer cast
660 after corrections for volume and water replenishment following sampling. Error bars mark the
661 deviations from the mean of the measurements in the two cores.

662

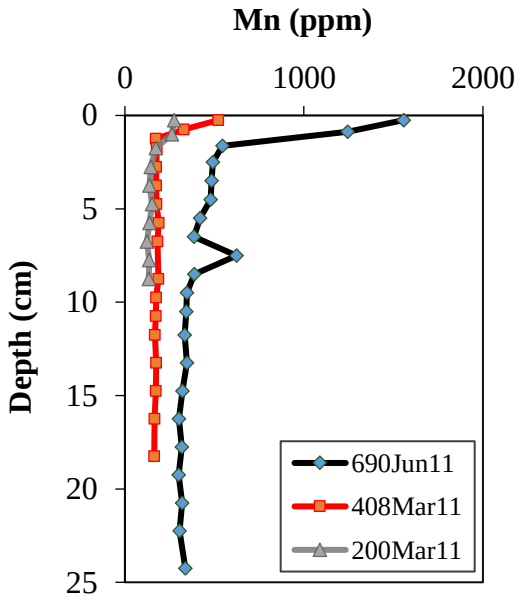

663

664 Fig. 11: Solid phase manganese extracted by 4M HNO_3.

665 **Table 1:** Common redox reactions in the upper marine sediment column and their
666 stoichiometric effect on total alkalinity (A_T) and dissolved inorganic carbon (DIC) per mole
667 reactant (Formulated after Boudreau, 1996; Cai et al., 2010; Krumins et al., 2013):

Redox Reactions		**DIC**	**A_T**
(R1)	$OM + 138O_2 \rightarrow 106CO_2 + 122H_2O + 16NO_3^- + H_2PO_4^- + 17H^+$	$+1$	$-17/106$
(R2)	$OM + 0.8 \cdot 106NO_3^- \rightarrow 106CO_2 + 0.4 \cdot 106N_2 + 16NH_4^+ + H_2PO_4^- + 48.6H_2O + (0.8 \cdot 106 + 15)OH^-$	$+1$	$+99.8/106$
(R3)	$OM + 2 \cdot 106MnO_2 + 121H_2O \rightarrow 106CO_2 + 16NH_4^+ + H_2PO_4^- + 2 \cdot 106Mn^{2+} + (4 \cdot 106 + 15)OH^-$	$+1$	$+439/106$
(R4)	$OM + 4 \cdot 106FeOOH + 121H_2O \rightarrow 106CO_2 + 16NH_4^+ + H_2PO_4^- + 4 \cdot 106Fe^{2+} + (8 \cdot 106 + 15)OH^-$	$+1$	$+863/106$
(R5)	$OM + 53SO_4^- + 15H^+ \rightarrow 53H_2S + 106HCO_3^- + 16NH_4^+ + H_2PO_4^-$	$+1$	$+121/106$
(R6)	$NH_4^+ + 2O_2 \rightarrow NO_3^- + H_2O + 2H^+$	0	-2
(R7)	$Mn^{2+} + 0.5O_2 + H_2O \rightarrow MnO_2 + 2H^+$	0	-2
(R8)	$Fe^{2+} + 0.25O_2 + 1.5H_2O \rightarrow FeOOH + 2H^+$	0	-2
(R9)	$H_2S + 2O_2 \rightarrow SO_4^{2-} + 2H^+$	0	-2
(R10)	$Fe^{2+} + 0.5MnO_2 + H_2O \rightarrow 0.5Mn^{2+} + FeOOH + H^+$	0	-1
(R11)	$H_2S + 4MnO_2 + 6H^+ \rightarrow SO_4^{2-} + 4Mn^{2+} + 4H_2O$	0	$+6$

668 * $OM \equiv (CH_2O)_{106}(NH_3)_{16}H_3PO_4$, assuming Redfield stoichiometry.

Cited Literature

Aller, R.C. (2014) Sedimentary diagenesis, depositional environments, and benthic fluxes, in: Holland, H.D., Turekian, K.K. (Eds.), Treatise on Geochemistry, 2nd ed. Elsevier, Oxford, pp. 293-334.

Almogi-Labin, A., Hemleben, C. and Meischner, D. (1998) Carbonate preservation and climatic changes in the central Red Sea during the last 380 kyr as recorded by pteropods. Marine Micropaleontology 33, 87-107.

Archer, D., Emerson, S. and Reimers, C. (1989) Dissolution of calcite in deep sea sediments: pH and O_2 microelectrode results. Geochimica et Cosmochimica Acta 53, 2831-2845.

Armstrong, R.A., Lee, C., Hedges, J.I., Honjo, S. and Wakeham, S.G. (2002) A new, mechanistic model for organic carbon fluxes in the ocean based on the quantitative association of POC with ballast minerals. Deep-Sea Research Part II-Topical Studies in Oceanography 49, 219-236.

Berelson, W.M., Balch, W.M., Najjar, R., Feely, R.A., Sabine, C. and Lee, K. (2007) Relating estimates of $CaCO_3$ production, export, and dissolution in the water column to measurements of $CaCO_3$ rain into sediment traps and dissolution on the sea floor: A revised global carbonate budget. Global Biogeochemical Cycles 21, 15.

Berelson, W.M., Hammond, D.E. and Cutter, G.A. (1990) In situ measurements of calcium carbonate dissolution rates in deep-sea sediments. Geochimica et Cosmochimica Acta 54, 3013-3020.

Berg, P., Risgaard-Petersen, N. and Rysgaard S. (1998) Interpretation of measured concentration profiles in sediment pore water. Limnology and Oceanography 43(7), 1500-1510.

Biton, E. and Gildor, H. (2011) The general circulation of the Gulf of Aqaba (Gulf of Eilat) revisited: The interplay between the exchange flow through the Straits of Tiran and surface fluxes. Journal of Geophysical Research-Oceans 116, 15.

Black, K.D., Calder, L.A., Nickell, T.D., Sayer, M.D.J., Orr, H., Brand, T., Cook, E.J., Magill, S.H., Katz, T., Eden, N., Jones, K.J., Tsapakis, M. and Angel, D. (2012) Chlorophyll, lipid profiles and bioturbation in sediments around a fish cage farm in the Gulf of Eilat, Israel. Aquaculture 356, 317-327.

Blonder, B., Boyko, V., Turchyn, A.V., Antler, G., Sinichkin, U., Knossow, N., Klein, R. and Kamyshny A. Jr. (2017) Impact of aeolian dry deposition of reactive iron minerals on sulfur cycling in sediments of the Gulf of Aqaba. Frontiers in Microbiology 8:1131.

Boudreau, B.P. (1996) A method-of-lines code for carbon and nutrient diagenesis in aquatic sediments. Computers & Geosciences 22, 479-496.

Boyko, V., Torfstein, A. and Kamyshny A. Jr. (2018) Oxygen consumption in permeable and cohesive sediments of the Gulf of Aqaba. Aquatic Geochemistry 24(3), 165-193.

Broecker, W.S. and Clark, E. (2003) Pseudo dissolution of marine calcite. Earth and Planetary Science Letters 208, 291-296.

Broecker, W.S. and Peng, T.-H. (1982) Tracers in the sea. The Lamont-Doherty Geological Observatory, Palisades, NY.

Broecker, W.S. and Peng, T.-H. (1974) Gas exchange rates between air and sea. Tellus 26, 21-35.

Burdige, D.J. (2006) Geochemistry of marine sediments. Princeton University Press, Princeton, NJ.

Cai, W.J., Chen, F.Z., Powell, E.N., Walker, S.E., Parsons-Hubbard, K.M., Staff, G.M., Wang, Y.C., Ashton-Alcox, K.A., Callender, W.R. and Brett, C.E. (2006) Preferential dissolution of carbonate shells driven by petroleum seep activity in the Gulf of Mexico. Earth and Planetary Science Letters 248, 227-243.

Cai, W.J., Luther, G.W., III, Cornwell, J.C. and Giblin, A.E. (2010) Carbon cycling and the coupling between proton and electron transfer reactions in aquatic sediments in Lake Champlain. Aquatic Geochemistry 16, 421-446.

Canfield, D.E., Thamdrup, B. and Hansen, J.W. (1993) The anaerobic degradation of organic matter in Danish coastal sediments: Iron reduction, manganese reduction, and sulfate reduction. Geochimica et Cosmochimica Acta 57, 3867-3883.

Chiu, T.C. and Broecker, W.S. (2008) Toward better paleocarbonate ion reconstructions: New insights regarding the $CaCO_3$ size index. Paleoceanography 23, 7.

Dickson, A.G. and Millero, F.J. (1987) A comparison of the equilibrium constants for the dissociation of carbonic acid in seawater media. Deep-Sea Research Part A-Oceanographic Research Papers 34, 1733-1743.

Doney, S.C., Fabry, V.J., Feely, R.A. and Kleypas, J.A. (2009) Ocean acidification: The other CO_2 problem, Annual Review of Marine Science, Palo Alto, pp. 169-192.

Dong, S., Subhas, A.V., Rollins, N.E., Naviaux, J.D., Adkins, J.F. and Berelson W.M (2018) A kinetic pressure effect on calcite dissolution in seawater. Geochimica et Cosmochimica Acta 238, 411-423.

Drupp, P.S., De Carlo, E.H. and Mackenzie, F.T. (2016) Porewater CO_2-carbonic acid system chemistry in permeable carbonate reef sands. Marine Chemistry 185, 48-64.

Emerson, S. and Bender, M. (1981) Carbon fluxes at the sediment-water interface of the deep-sea - calcium-carbonate preservation. Journal of Marine Research 39, 139-162.

Engel, A., Abramson, L., Szlosek, J., Liu, Z., Stewart, G., Hirschberg, D. and Lee, C. (2009) Investigating the effect of ballasting by $CaCO_3$ in *Emiliania huxleyi*, II: Decomposition of particulate organic matter. Deep Sea Research Part II 56(18), 1408-1419.

Epping, E., van der Zee, C., Soetaert, K. and Helder, W. (2002) On the oxidation and burial of organic carbon in sediments of the Iberian margin and Nazare Canyon (NE Atlantic). Progress in Oceanography 52, 399-431.

Feely, R.A., Sabine, C.L., Lee, K., Berelson, W., Kleypas, J., Fabry, V.J. and Millero, F.J. (2004) Impact of anthropogenic CO_2 on the $CaCO_3$ system in the oceans. Science 305, 362-366.

Freiwald, A. (1995) Bacteria-induced carbonate degradation: A taphonomic case study of cibicides lobatulus from a high-boreal carbonate setting. Palaios 10, 337-346.

Froelich, P.N., Klinkhammer, G.P., Bender, M.L., Luedtke, N.A., Heath, G.R., Cullen, D., Dauphin, P., Hammond, D., Hartman, B. and Maynard, V. (1979) Early oxidation of organic matter in pelagic sediments of the eastern equatorial Atlantic: Suboxic diagenesis. Geochimica et Cosmochimica Acta 43, 1075-1090.

Glud, R.N. (2008) Oxygen dynamics of marine sediments. Marine Biology Research 4, 243-289.

Glud, R.N., Gundersen, J.K., Jorgensen, B.B., Revsbech, N.P. and Schulz, H.D. (1994) Diffusive and total oxygen uptake of deep-sea sediments in the eastern South Atlantic Ocean: *in situ* and laboratory measurements. Deep-Sea Research Part I-Oceanographic Research Papers 41, 1767-1788.

Green, M.A. and Aller, R.C. (2001) Early diagenesis of calcium carbonate in Long Island Sound sediments: Benthic fluxes of Ca^{2+} and minor elements during seasonal periods of net dissolution. Journal of Marine Research 59, 769-794.

Gupta, A.K., Anderson, D.M. and Overpeck, J.T. (2003) Abrupt changes in the Asian southwest monsoon during the Holocene and their links to the North Atlantic Ocean. Nature 421, 354-357.

Hales, B. (2003) Respiration, dissolution, and the lysocline. Paleoceanography 18, 14.

Hales, B. and Emerson, S. (1997) Evidence in support of first-order dissolution kinetics of calcite in seawater. Earth and Planetary Science Letters 148, 317-327.

Hales, B., Emerson, S. and Archer, D. (1994) Respiration and dissolution in the sediments of the western North-Atlantic: estimates from models of in situ microelectrode measurements of porewater oxygen and pH. Deep-Sea Research Part I-Oceanographic Research Papers 41, 695-719.

Hansen, H.P. and Koroleff, F. (1999) Determination of nutrients, in: Grasshoff, K., Kremling, K., Ehrhardt, M. (Eds.), Methods of Seawater Analyses, 3rd ed. Wiley-VCH, Weinheim, pp. 159-228.

Harris, R.P. (1994) Zooplankton grazing on the coccolithophore Emiliania huxleyi and its role in inorganic carbon flux. Marine Biology 119, 431-439.

Holmes, R.M., Aminot, A., Kérouel, R., Hooker, B.A. and Peterson, B.J. (1999) A simple and precise method for measuring ammonium in marine and freshwater ecosystems. Canadian Journal of Fisheries and Aquatic Sciences 56, 1801-1808.

Hu, X.P. and Burdige, D.J. (2007) Enriched stable carbon isotopes in the pore waters of carbonate sediments dominated by seagrasses: Evidence for coupled carbonate dissolution and reprecipitation. Geochimica et Cosmochimica Acta 71, 129-144.

Ilyina, T. and Zeebe, R.E. (2012) Detection and projection of carbonate dissolution in the water column and deep-sea sediments due to ocean acidification. Geophysical Research Letters 39, 6.

Jahnke, R.A., Craven, D.B., McCorkle, D.C. and Reimers, C.E. (1997) $CaCO_3$ dissolution in California continental margin sediments: The influence of organic matter remineralization. Geochimica et Cosmochimica Acta 61, 3587-3604.

Jahnke, R.A. and Jahnke, D.B. (2004) Calcium carbonate dissolution in deep sea sediments: Reconciling microelectrode, pore water and benthic flux chamber results. Geochimica et Cosmochimica Acta 68, 47-59.

Johnson, K.S. (1982) Solubility of rhodochrosite ($MnCO_3$) in water and seawater. Geochimica et Cosmochimica Acta 46, 1805-1809.

Jourabchi, P., Van Cappellen, P. and Regnier, P. (2005) Quantitative interpretation of pH distributions in aquatic sediments: A reaction-transport modeling approach. American Journal of Science 305, 919-956.

Keil, R. (2017) Anthropogenic forcing of carbonate and organic carbon preservation in marine sediments. Annual Review of Marine Science 9, 151-172.

Klaas, C. and Archer, D.E. (2002) Association of sinking organic matter with various types of mineral ballast in the deep sea: Implications for the rain ratio. Global Biogeochemical Cycles 16, 14.

Krumgalz, B.S. and Erez, J. (1984) Chemical oceanography survey of the northern Red Sea, the straits of Tiran and the Gulf of Elat. I.O.L.R. reports, series H.

Krumgalz, B.S., Erez, J. and Chen, C.T.A. (1990) Anthropogenic CO_2 penetration in the northern Red Sea and in the Gulf of Elat (Aqaba). Oceanologica Acta 13, 283-290.

Krumins, V., Gehlen, M., Arndt, S., Van Cappellen, P. and Regnier, P. (2013) Dissolved inorganic carbon and alkalinity fluxes from coastal marine sediments: model estimates for different shelf environments and sensitivity to global change. Biogeosciences 10, 371-398.

Lazar, B., Erez, J., Silverman, J., Rivlin, T., Rivlin, A., Dray, M., Meeder, E. and Iluz, D. (2008) Recent environmental changes in the chemical-biological oceanography of the Gulf of Aqaba (Eilat), in: Por, F.D. (Ed.), Aqaba-Eilat, the improbable gulf. Environment, biodiversity and preservation. Magnes Press, Jerusalem.

Le Quéré, C., Andrew, R. M., Friedlingstein, P., Sitch, S., Pongratz, J., Manning, A. C., Korsbakken, J. I., Peters, G. P., Canadell, J. G., Jackson, R. B., Boden, T. A., Tans, P. P., Andrews, O. D., Arora, V. K., Bakker, D. C. E., Barbero, L., Becker, M., Betts, R. A., Bopp, L., Chevallier, F., Chini, L. P., Ciais, P., Cosca, C. E., Cross, J., Currie, K., Gasser, T., Harris, I., Hauck, J., Haverd, V., Houghton, R. A., Hunt, C. W., Hurtt, G., Ilyina, T., Jain, A. K., Kato, E., Kautz, M., Keeling, R. F., Klein Goldewijk, K., Körtzinger, A., Landschützer, P., Lefèvre, N., Lenton, A., Lienert, S., Lima, I., Lombardozzi, D., Metzl,

N., Millero, F., Monteiro, P. M. S., Munro, D. R., Nabel, J. E. M. S., Nakaoka, S.-I., Nojiri, Y., Padin, X. A., Peregon, A., Pfeil, B., Pierrot, D., Poulter, B., Rehder, G., Reimer, J., Rödenbeck, C., Schwinger, J., Séférian, R., Skjelvan, I., Stocker, B. D., Tian, H., Tilbrook, B., Tubiello, F. N., van der Laan-Luijkx, I. T., van der Werf, G. R., van Heuven, S., Viovy, N., Vuichard, N., Walker, A. P., Watson, A. J., Wiltshire, A. J., Zaehle, S., and Zhu, D. (2018) Global Carbon Budget 2017. Earth Syst. Sci. Data, 10, 405-448.

Lee, K., Kim, T.-W., Byrne, R.H., Millero, F.J., Feely, R.A. and Liu, Y.-M. (2010) The universal ratio of boron to chlorinity for the North Pacific and North Atlantic oceans. Geochimica et Cosmochimica Acta 74, 1801-1811.

Lewis, E. and Wallace, D.W.R. (1998) Program Developed for CO_2 System Calculations. Carbon Dioxide Information Analysis Center, Oak Ridge National Laboratory, U.S. Department of Energy, Oak Ridge, Tennessee.

Li, Y.H. and Gregory, S. (1974) Diffusion of ions in sea water and in deep-sea sediments. Geochimica et Cosmochimica Acta 38, 703-714.

Martin, W.R. and Sayles, F.L. (2006) Organic matter oxidation in deep-sea sediments: Distribution in the sediment column and implications for calcite dissolution. Deep-Sea Research Part II-Topical Studies in Oceanography 53, 771-792.

McBride, M.B., 1979. Chemisorption and precipitation of Mn^{2+} at $CaCO_3$ surfaces. Soil Sci. Soc. Am. J. 43, 693-698.

Meeder, E., Mackey, K.R.M., Paytan, A., Shaked, Y., Iluz, D., Stambler, N., Rivlin, T., Post, A.F. and Lazar, B. Nitrite dynamics in the open ocean - clues from seasonal and diurnal variations. Marine Ecology Progress Series 453, 11-26.

Mehrbach, C., Culberson, C.H., Hawley, J.E. and Pytkowicz, R.M. (1973) Measurement of the apparent dissociation constants of carbonic acid in seawater at atmospheric pressure. Limnology and Oceanography 18, 897-907.

Middelburg, J.J., de Lange, G.J. and van der Weijden, C.H. (1987) Manganese solubility control in marine pore waters. Geochimica et Cosmochimica Acta 51, 759-763.

Millero, F.J. (1995) Thermodynamics of the carbon dioxide system in the oceans. Geochimica et Cosmochimica Acta 59, 661-677.

Morse, J.W., Andersson, A.J. and Mackenzie, F.T. (2006) Initial responses of carbonate-rich shelf sediments to rising atmospheric pCO_2 and "ocean acidification": Role of high Mg-calcites. Geochimica et Cosmochimica Acta 70, 5814-5830.

Mucci, A. (1983) The solubility of calcite and aragonite in seawater at various salinities, temperatures, and one atmosphere total pressure. American Journal of Science 283, 780-799.

Mucci, A. (1988) Manganese uptake during calcite precipitation from seawater: Conditions leading to the formation of a pseudokutnahorite. Geochimica et Cosmochimica Acta 52, 1859-1868.

Orr, J.C., Fabry, V.J., Aumont, O., Bopp, L., Doney, S.C., Feely, R.A., Gnanadesikan, A., Gruber, N., Ishida, A., Joos, F., Key, R.M., Lindsay, K., Maier-Reimer, E., Matear, R., Monfray, P., Mouchet, A., Najjar, R.G., Plattner, G.K., Rodgers, K.B., Sabine, C.L., Sarmiento, J.L., Schlitzer, R., Slater, R.D., Totterdell, I.J., Weirig, M.F., Yamanaka, Y. and Yool, A. (2005) Anthropogenic ocean acidification over the twenty-first century and its impact on calcifying organisms. Nature 437, 681-686.

Parkhurst, D.L. and Appelo, C.A.J. (2013) Description of input and examples for PHREEQC version 3--A computer program for speciation, batch- reaction, one-dimensional transport, and inverse geochemical calculations, U.S. Geological Survey Techniques and Methods, book 6, p. 497.

Pierrot, D., Lewis, E. and Wallace, D.W.R. (2006) MS Excel program developed for CO_2 system calculations. ORNL/CDIAC-105a. Carbon Dioxide Information Analysis Center, Oak Ridge National Laboratory, U.S. Department of Energy, Oak Ridge, Tennessee.

Raven, J., Caldeira, K., Elderfield, H., Hoegh-Guldberg, O., Liss, P., Riebesell, U., Sheperd, J., Turley, C. and Watson, A. (2005) Ocean acidification due to increasing atmospheric carbon dioxide. Royal Society, London.

Redfield, A.C. (1958) The biological control of chemical factors in the environment. American Scientist 46, 205-221.

Ries, J.B., Ghazaleh, M.N., Connolly, B., Westfield, I. and Castillo, K.D. (2016) Impacts of seawater saturation state (Omega(A)=0.4-4.6) and temperature (10, 25 degrees C) on the dissolution kinetics of whole-shell biogenic carbonates. Geochimica et Cosmochimica Acta 192, 318-337.

Sabine, C.L., Feely, R.A., Gruber, N., Key, R.M., Lee, K., Bullister, J.L., Wanninkhof, R., Wong, C.S., Wallace, D.W.R., Tilbrook, B., Millero, F.J., Peng, T.H., Kozyr, A., Ono, T. and Rios, A.F. (2004) The oceanic sink for anthropogenic CO_2. Science 305, 367-371.

Sass, E. and Ben-Yaakov, S. (1977) The carbonate system in hypersaline solutions: Dead Sea brines. Marine Chemistry 5, 183-199.

Silverman, J., Schneider, K., Kline, D.I., Rivlin, T., Rivlin, A., Hamylton, S., Lazar, B., Erez, J. and Caldeira, K. (2014) Community calcification in Lizard Island, Great Barrier Reef: A 33 year perspective. Geochimica et Cosmochimica Acta 144, 72-81.

Soetaert, K., Hofmann, A.F., Middelburg, J.J., Meysman, F.J.R. and Greenwood, J. (2007) The effect of biogeochemical processes on pH. Marine Chemistry 105, 30-51.

Sofianos, S.S. and Johns, W.E. (2002) An Oceanic General Circulation Model (OGCM) investigation of the Red Sea circulation, 1. Exchange between the Red Sea and the Indian Ocean. Journal of Geophysical Research-Oceans 107, 11.

Steiner, Z., Erez, J., Shemesh, A., Yam, R., Katz, A. and Lazar, B. (2014) Basin-scale estimates of pelagic and coral reef calcification in the Red Sea and Western Indian Ocean. Proceedings of the National Academy of Sciences of the United States of America 111, 16303-16308.

Steiner, Z., Lazar, B., Levi, S., Tsroya, S., Pelled, O., Bookman, R. and Erez, J. (2016) The effect of bioturbation in pelagic sediments: Lessons from radioactive tracers and planktonic foraminifera in the Gulf of Aqaba, Red Sea. Geochimica et Cosmochimica Acta 194, 139-152.

Steiner, Z., Lazar, B., Torfstein, A. and Erez, J. (2017) Testing the utility of geochemical proxies for paleoproductivity in oxic sedimentary settings of the Gulf of Aqaba, Red Sea. Chemical Geology 473, 40-49.

Steiner Z., Lazar B., Erez J. and Turchyn A.V. (2018a) Comparing Rhizon samplers and centrifugation for porewater separation in studies of the marine carbonate sediments. Limnology and Oceanography: Methods.

Steiner Z., Turchyn A.V., Harpaz E. and Silverman J. (2018b) Water chemistry reveals a significant decline in coral calcification rates in the southern Red Sea. Nature Communications, 9:3615.

Sultan, S. (2014) Global and local anthropogenic influences on the recent sedimentary record of the Gulf of Eilat, Institute of Earth Sciences. The Hebrew University, Jerusalem, p. 71.

Sun, X.L. and Turchyn, A.V. (2014) Significant contribution of authigenic carbonate to marine carbon burial. Nature Geoscience 7, 201-204.

Tibor, G., Niemi, T.M., Ben-Avraham, Z., Al-Zoubi, A., Sade, R.A., Hall, J.K., Hartman, G., Akawi, E., Abueladas, A. and Al-Ruzouq, R. (2010) Active tectonic morphology and submarine deformation of the northern Gulf of Eilat/ Aqaba from Analyses of multibeam data. Geo-Marine Letteres 30(6), 561-573.

Traub, E. (1985) Bacterial oxidation of organic matter in marine sediments and its effect on the carbonate system. The Hebrew University, Jerusalem.

898 Wartel, M., Skiker, M., Auger, Y. and Boughriet, A., (1990). Interaction of manganese(II) with
899 carbonates in seawater: assessment of the solubility product of $MnCO_3$ and Mn distribution coefficient
900 between the liquid phase and $CaCO_3$ particles. Marine Chemistry 29, 99-117.

901 Wurgaft, E., Steiner, Z., Luz, B. and Lazar, B. (2016) Evidence for inorganic precipitation of $CaCO_3$
902 on suspended solids in the open water of the Red-Sea. Marine Chemistry 186, 145-155.

903 Zeebe, R.E. (2011) On the molecular diffusion coefficients of dissolved CO_2, HCO_3^-, and CO_3^{2-} and
904 their dependence on isotopic mass. Geochimica et Cosmochimica Acta 75, 2483-2498.

905